Rh-Doped ZnO Monolayer as a Potential Gas Sensor for Air Decomposed Species in a Ring Main Unit: A First-Principles Study

Yan Wang, Xin Yang, Cong Hu, and Tian Wu*
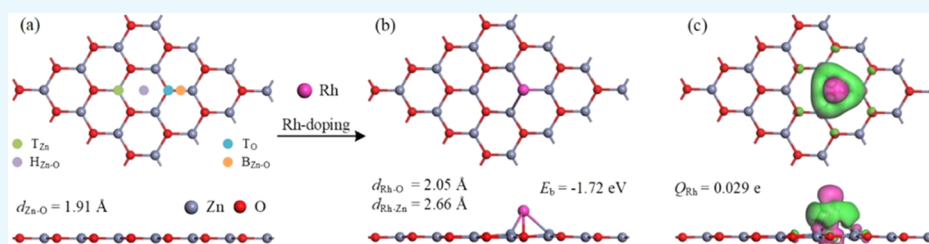
ACCESS | Metrics & More | Article Recommendations

ABSTRACT: Using the first-principles theory, this paper studies the Rh-doping behavior on the ZnO monolayer and investigates the adsorption and sensing behaviors of a Rh-doped ZnO (Rh−ZnO) monolayer to NO_2 and O_3 to explore its potential as a gas sensor to evaluate the operation status of the ring main unit in the power system. The results indicate that the Rh dopant can be stably anchored on the T_O site of the ZnO monolayer with an E_b of −2.11 eV. The Rh−ZnO monolayer shows chemisorption of NO_2 and O_3, with E_{ad} values of −2.11 and −1.35 eV, respectively. Then, the electronic behavior of the Rh−ZnO monolayer before and after gas adsorption is analyzed in detail to uncover the sensing mechanism for gas detection. Our findings indicate that the Rh−ZnO monolayer is a promising resistance-type gas sensor with a higher response to O_3 and can be explored as a field-effect gas sensor with a higher response to NO_2. Our theoretical calculations provide the basic sensing mechanism of the Rh−ZnO monolayer for gas detection and would be meaningful to explore novel sensing materials for gas detection in the field of electrical engineering.

1. INTRODUCTION

In the power system, the ring main unit is the widely applied equipment for electric transmission and distribution, with the advantages of simple operation, small size, and low cost.[1,2] From another aspect, safe operation plays a critical role in ensuring the safety and stability of the whole power system. When insulation defects such as partial discharge and partial overheat occur, the air in the ring main unit would be decomposed into several impurity gases wherein O_3 and NO_2 are the main species.[3,4] As reported, the presence of these decomposed species would impair the insulation behavior of the filled air, thus weakening the operation status of the ring main unit.[5] In the long run, the insulation defects would be disruptive and cause some accidents including line tripping and power cut.[6] Therefore, online monitoring of the operation status is important to ensure daily smooth running. For this purpose, the detection of air decomposed species, including O_3 and NO_2, is suggested to reflect the severity of the partial discharge and to evaluate the operation status of the ring main unit.[7] This until now is a widely applied approach to guarantee the safe operation of the whole power system.

The nanosensing method for gas detection is a workable manner with advantages of rapid response, high sensitivity, and low cost.[8−10] With the exploration of novel 2D materials, numerous candidates are proposed for gas sensing application

in many fields.[11−15] Recently, the II−VI semiconductor ZnO has attracted remarkable attention, owing to its large surface area and electronic motion.[16] Moreover, the graphene-like ZnO monolayer is explored and has been theoretically investigated with unique electronic and optical properties,[17,18] which provides the possibility to explore the ZnO monolayer as a potential chemical sensor for gas detection in many fields. For example, Han and Lee[19] studied the Ni-doped ZnO monolayer as a promising gas sensor for the detection of SF_6 decomposed species, wherein the Ni atom as a transition metal (TM) is selected as the dopant, meaning to promote the chemical reactivity of the whole system and improve the adsorption performance of the ZnO monolayer. Therefore, the TM-doped ZnO monolayer in our opinion would be a promising gas sensing material for gas detection, which should be investigated and could provide a solution for our issue.
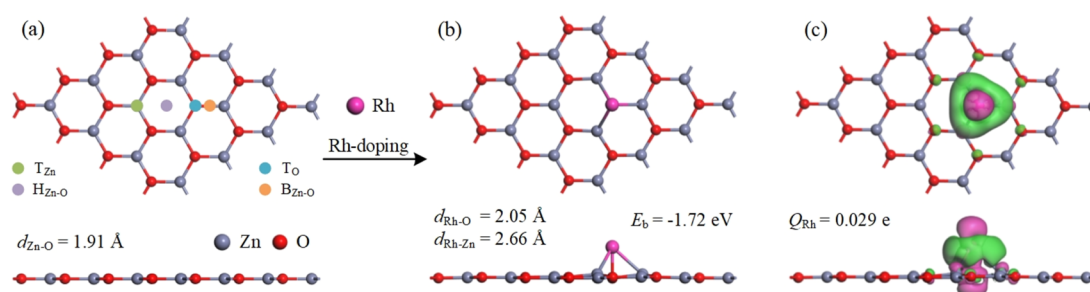
Figure 1. Rh-doping process on the ZnO monolayer. (a) Top and side views of the pristine ZnO monolayer. (b, c) MSC of the Rh−ZnO monolayer and the related CDD from the top and side views. In the CDD, the pink area is electron depletion, while the green area is electron accumulation, with the isosurface set as 0.01 e/Å^3.
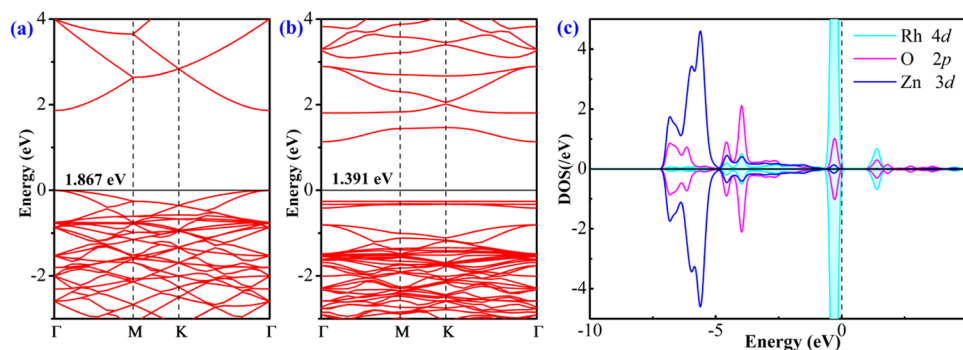

Figure 2. (a, b) BS of the pristine and Rh-doped ZnO monolayers and (c) orbital DOS of the Rh−ZnO system. In BS, the black values are band gaps of related systems, and in DOS, the Fermi level is set to zero.

In this work, a Rh-doped ZnO (Rh−ZnO) monolayer is proposed to theoretically investigate its adsorption and sensing behaviors to two air decomposed species (NO$_2$ and O$_3$) based on the first-principles theory. The Rh metal is widely applied as a TM dopant and is well behaved in some gas interactions due to its high catalytic property,[20−22] and it is our hope that Rh-doping can provide good performances for the ZnO system upon gas adsorption and sensing. Section 2 analyzes the Rh-doping behavior on the ZnO monolayer and the adsorption behavior as well sensor exploration for the Rh−ZnO monolayer, Section 3 puts forward the main conclusions, and Section 4 gives the computational details of the calculations.

2. RESULTS AND DISCUSSION

2.1. Rh-Doping Behavior on the ZnO Monolayer. The Rh-doping process is performed on the optimized structure of a pristine 4 × 4 × 1 ZnO supercell, as plotted in Figure 1a (top and side views) with possible doping sites. One can see that the ZnO monolayer displays a graphene-like structure and the Zn−O bond is measured to be 1.91 Å. Based on our calculations, the lattice constant of the optimized ZnO monolayer is found to be 3.30 Å in this work. These findings are in good agreement with ref 23, indicating the good accuracy of our calculations. In terms of Rh-doping on the pristine ZnO surface, four possible sites are considered, traced as T$_{Zn}$ (on top of the Zn atom), H$_{Zn−O}$ (on top of the hexatomic Zn−O ring), T$_O$ (on top of the O atom), and B$_{Zn−O}$ (on the bridge of the Zn−O bond).

The most stable configuration (MSC) of the Rh−ZnO monolayer is plotted in Figure 1b with the related charge density difference (CDD) shown in Figure 1c. It is found that among the four possible sites, the preferred Rh-doping site on the pristine ZnO monolayer is the T$_O$ site, on which the Rh

dopant forms a tripod-like structure with three Zn atoms and is bonded with the O atom as well. E_b for Rh-doping through the T$_O$ site is calculated to be −1.72 eV, much larger than that through the T$_{Zn}$ site (−0.78 eV). Interestingly, the optimized structures of the Rh-doping process through the H$_{Zn−O}$ and B$_{Zn−O}$ sites would be equivalent to that through the T$_O$ site, where apparently the atomic displacement of the Rh dopant could be verified. Moreover, vibrational analysis shows that the frequencies of the Rh−ZnO monolayer range from 43.11 to 1349.83 cm^{-1}, which confirms its good chemical stability.[24] These results show the strong binding force of the Rh dopant with the ZnO surface, especially on the T$_O$ site that leads to the formation of the Rh−O and Rh−Zn bonds measured to be 2.05 and 2.66 Å, respectively.

According to the Hirshfeld analysis, the Rh dopant is positively charged by 0.029e in the Rh−ZnO system, which indicates that the Rh dopant contributes 0.029e to the ZnO monolayer during doping. This suggests the electron-losing property of the Rh dopant when interacting with the ZnO surface and agrees with those of other nanosurfaces, as reported in refs 25, 26. From the Pauling electronegativity, it is known that the electronegativity of the Rh dopant (2.20) is between those of the Zn and O atoms (1.65 and 3.44,[27] respectively). That is, the Rh dopant is supposed to trap electrons from the Zn atom and donate electrons to the O atom during the formation of new bonds. Since the Rh dopant is positively charged in the Rh−ZnO system, it could be assumed that the Rh dopant has a stronger interaction with the O atom compared with the Zn atom. This finding supports the larger E_b for Rh-doping on the T$_O$ site compared with the T$_{Zn}$ site as well as the stronger binding force of the Rh−O bond compared with the Rh−Zn bond. From the CDD, we can see that the Rh dopant is mainly embraced by electron depletion,
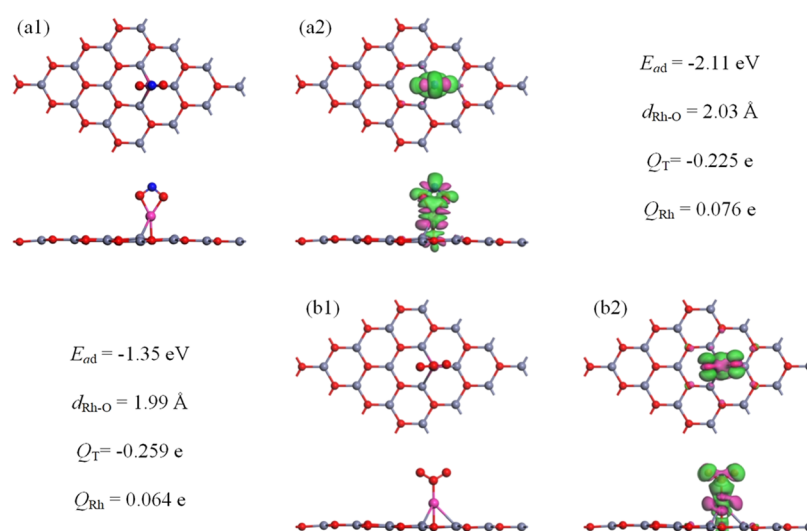
Figure 3. MSC and CDD for (a) NO_2 and (b) O_3 adsorption on the Rh–ZnO monolayer. The set in the CDD is same as Figure 1.

while the Rh–Zn and Rh–O bonds are mainly embraced by electron accumulation. These results manifest the electron-releasing property of the Rh dopant and the strong electron hybridization on the Rh–Zn and Rh–O bonds that results in their strong binding force and related E_b for the Rh–ZnO system.

To further comprehend the Rh-doping behavior on the electronic property of the ZnO monolayer, we calculate the band structure (BS) of the pristine and Rh-doped ZnO systems for comparison, as plotted in Figure 2a,b. Besides, the orbital density of state (DOS) between the Rh dopant and O as well as Zn atoms is plotted in Figure 2c to show their orbital interaction during doping. Based on our calculations, the band gap of the pristine ZnO monolayer is obtained as 1.867 eV, which agrees with the previous reports, suggesting the good accuracy of our calculations.[18] Besides, the top of the valence band and the bottom of the conduction band are both localized at the Γ points, verifying its direct semiconducting property. After Rh-doping, the band gap of the Rh–ZnO system is narrowed to 1.391 eV and the state distribution becomes denser, which can be attributed to the Rh-doping behavior that induces many novel states for the Rh-doped system and several impurity states within the band gap of the pristine ZnO system. Apart from this, the top of the valence band is localized at the k-point, while the bottom of the valence band is localized at the Γ point, which manifests the indirect semiconducting property for the Rh–ZnO system, resulting from the impurity state induced by Rh-doping. Also, such an indirect semiconducting property suggests the unsuitability of the Rh–ZnO monolayer for optical applications in some fields.[28] From Figure 2c where the orbital DOS of bonded atoms is displayed, it is found that the Rh 4d orbital is highly hybrid with the O 2p orbital at −4.5, −4.0, −0.3, and 1.4 eV, while has little hybridization with the Zn 3d orbital. These findings verify the stronger binding force of the Rh–O bond compared with that of the Rh–Zn bond.

2.2. Gas Adsorption Behavior. With the optimized Rh–ZnO monolayer, the adsorption of NO_2 and O_3 is conducted to analyze its potential as a gas sensor. To establish the gas adsorption systems, the gas species approach the Rh center appropriately 3 Å in various configurations to study different atomic interactions with the Rh dopant. With fully geometric

optimization, the MSC for gas adsorption with the lowest E_{ad} is portrayed in Figure 3. Also, some important adsorption parameters are also listed in this figure for better understanding and analysis.

For NO_2 adsorption on the Rh–ZnO surface, it is seen that the NO_2 molecule is vertical to the ZnO layer and seems to be standing on top of the Rh dopant through the O-end position, and two O atoms of the NO_2 molecule are captured by the Rh dopant forming two Rh–O bonds with lengths of 2.03 and 2.05 Å, respectively. At the same time, the geometric structure of the Rh–ZnO monolayer undergoes some deformations after NO_2 adsorption. In detailed, one Rh–Zn bond is broken and the other two Rh–Zn bonds are elongated to 2.73 and 2.74 Å, respectively; in addition, the Rh–O bond of the Rh–ZnO monolayer is slanting slightly with an elongated length of 2.08 Å, making the Rh–O bond not vertical to the ZnO layer. E_{ad} in this system is calculated to be −2.11 eV, which indicates the strong binding force between the Rh dopant and the O atom of the NO_2 molecule that causes the chemisorption for NO_2 adsorption on the Rh–ZnO surface.[29] According to the Hirshfeld analysis, NO_2 after adsorption as a whole accepts 0.225e from the Rh–ZnO monolayer, and the Rh dopant is positively charged by 0.076e. These results present that the Rh dopant transfers 0.047e to NO_2, while the ZnO surface through the Rh dopant transfers 0.178e to NO_2. From the CDD, one can find that the electron accumulation is mainly localized on the newly formed Rh–O bonds, while the electron depletion is mainly localized on the Rh dopant and the Rh–O and Rh–Zn bonds of the Rh–ZnO monolayer, which agrees with the Hirshfeld analysis, indicating both remarkable electron redistribution and hybridization for the Rh–ZnO system caused by NO_2 adsorption.

When it comes to the O_3 system, one can see that the adsorption configuration is similar to that of the NO_2 system. However, the O_3 molecule is vertical with the ZnO layer and the middle O atom is trapped by the Rh dopant, with two O–O bonds pointing to the vacuum region instead of the Rh dopant. The newly formed Rh–O bond is measured to be 1.99 Å, and the Rh–O and Rh–Zn bonds of the Rh–ZnO monolayer are elongated to 2.07 and 2.80 Å, respectively. Besides, the E_{ad} in this system is calculated to be −1.35 eV. Although the chemisorption can also be identified in the O_3
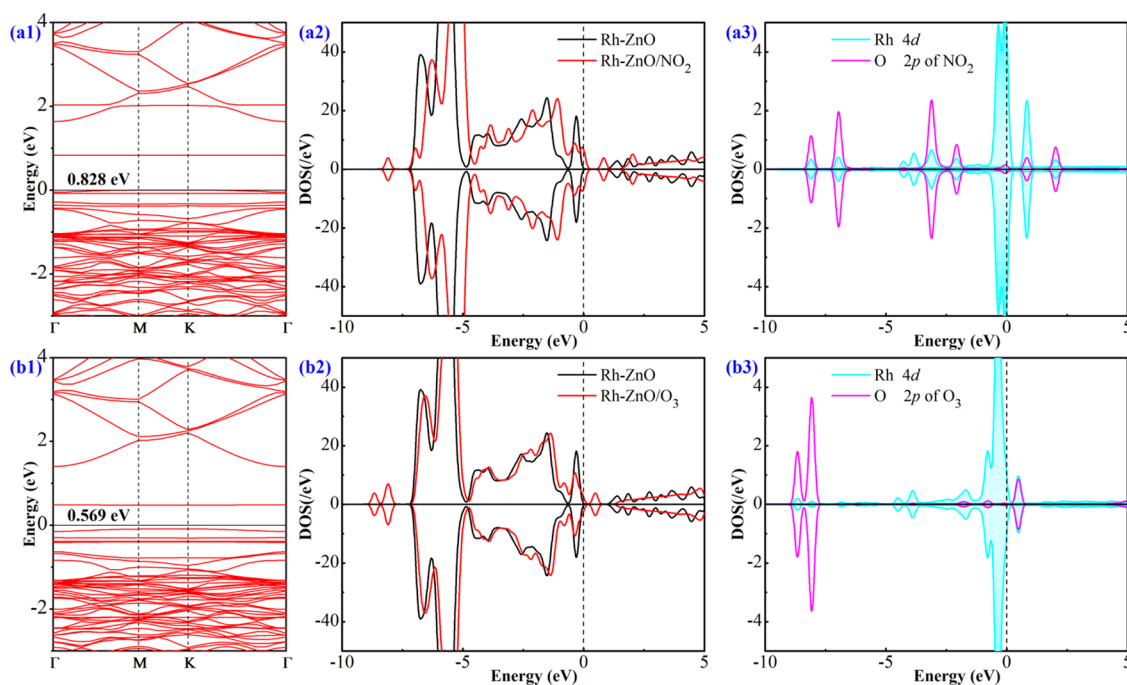
Figure 4. BS and DOS of gas adsorption systems. (a1–a3) NO_2 system and (b1–b3) O_3 system. In BS, the black values are band gaps of related systems, and in DOS, the Fermi level is set to zero.

system given the larger absolute value of E_{ad} here than the critical value (0.8 eV[30]), the adsorption strength is not larger than that in the NO_2 system. According to the Hirshfeld analysis, the Rh–ZnO monolayer transfers $0.259e$ to the O_3 molecule, and given the positively charged Rh dopant of $0.064e$, a Q_T of $0.035e$ is contributed by the Rh dopant. The significant charge transfer accounts for the electron redistribution in the O_3 system, as shown in the CDD wherein the strong electron accumulation is localized on the O_3 molecule and the newly formed Rh–O bond, while the electron deletion is on the Rh dopant and the Rh–O and Rh–Zn bonds of the Rh–ZnO monolayer.

In short, we can conclude from the above analysis that the Rh–ZnO monolayer shows stronger chemisorption of NO_2 than O_3, leading to the larger E_{ad} in the former system. Meanwhile, the Hirshfeld analysis indicates that both NO_2 than O_3 molecules behave as electron acceptors during their adsorption. This may be due to the larger electronegativity of the O atom (3.44) compared with the Rh dopant (2.20),[27] and the O atom of the adsorbed NO_2 or O_3 would attach the electron from the Rh dopant through the Rh–O bond. The electron redistribution can also modify the electronic behavior of the Rh–ZnO monolayer, which may expound the sensing mechanism for gas detection from the microperspective, which is further analyzed in the next section.

2.3. Electronic Behavior in Gas Systems. After the chemisorption of NO_2 and O_3, the electronic behavior of the Rh–ZnO monolayer would be somewhat modulated. To elaborate on the electronic deformations, the BS and DOS of the gas adsorption systems are calculated and displayed in Figure 4 for better comprehension.

For the BS of the NO_2 system, it is found that the band gap is narrowed to 0.828 eV from 1.391 eV in the isolated Rh–ZnO system, which can result from the states of the adsorbed NO_2 that induces some impurity states within the band gap of the Rh–ZnO monolayer. From the total DOS, one can see that

the induced impurity states are mainly localized at −8.1, −6.9, and 0.8 eV. Besides, the DOS curves of the NO_2 system are rightshifted compared with the pure Rh–ZnO system, which results from the electron-accepting behavior of NO_2 that reduces the energy of the Fermi level. A similar but not identical phenomenon can be found in the O_3 system as well. The band gap for the O_3 system is obtained as 0.569 eV, further smaller than the NO_2 system, implying the stronger deformation in the electronic behavior of the Rh–ZnO monolayer. This, to the best of our knowledge, may be due to larger Q_T that causes more efficient electron redistribution in the O_3 system. The total DOS illustrates that the states of the adsorbed O_3 are mainly localized at −8.6, −8.1, −2.2, −0.8, and 0.4 eV. Since the total DOS of the gas adsorbed system would be largely impacted by the state contributions of the adsorbed gas species, the DOS distribution in the O_3 system is thus tuned by the adsorbed O_3, especially by those states around the Fermi level. Given that the induced states around the Fermi level of the O_3 system are denser than those in the NO_2 system, it is predictable that the tuned electronic property of the Rh–ZnO monolayer would be stronger in the O_3 system, thus causing the larger decline in the band gap.

For the orbital DOS of the NO_2 and O_3 systems, one can observe that the orbital hybridizations between the Rh 4d and O 2p orbitals are mainly localized at −8.1, −6.9, −3.1, −2.1, 0.8, and 2.0 eV for the NO_2 system and −8.7, −8.1, −1.7, −0.8, and 0.4 eV for the O_3 system. Such state overlaps manifest the strong orbital interaction between the Rh dopant and the O atom of the adsorbed gas species, thereby leading to the formation of new chemical bonds and large E_{ad} in the two systems. In addition, the larger overlapped area between the DOS states of the Rh dopant and the O atom in the NO_2 system suggests the stronger binding force and supports the larger E_{ad} than that in the O_3 system. All these electronic analyses agree with the analyses of adsorption parameters well.

2.4. Exploration of the Gas Sensor. The change of band gap in the Rh−ZnO monolayer after gas adsorption accounts for the change of its electrical conductivity, which illustrates the sensing mechanism for NO_2 and O_3 detection and its potential to evaluate the operation status of the ring main units. It is well known that the electrical conductivity (σ) of materials is related to their band gap as[31]

$$\sigma \propto e^{(-B_g/2kT)} \tag{1}$$

where B_g is the related band gap, k is the Boltzmann constant, and T is the temperature. One can infer from this formula that large B_g would accord with smaller electrical conductivity, and the increase of B_g can lead to the decrease of electrical conductivity. Therefore, the electrical conductivity of the Rh−ZnO monolayer would be increased after adsorption of NO_2 and O_3. Besides, the changing rate of the band gap in the NO_2 and O_3 systems are calculated to be −40.5 and −59.1%, respectively. Therefore, it can be presumed that such obvious changes of the band gap in the Rh−ZnO monolayer after the adsorption of the two gases can lead to an admirable change of electrical resistance and then cause a detectable electrical response for sensitive measurement by resistance-detecting devices. In other words, the Rh−ZnO monolayer is of great potential to be explored as a resistance-type gas sensor for the detection of NO_2 and O_3, which provides a workable method to evaluate the operation status of the ring main unit in a simple manner. Note that in the single gaseous atmosphere, the Rh−ZnO monolayer can show a higher sensing response to O_3 compared with NO_2 as a resistance-type gas sensor.

Given the apparent change of the band gap for the Rh−ZnO monolayer for gas detection, we assume it would also be a good candidate for exploration as a field-effect transistor gas sensor by which the gas sensitivity would become much higher and the sensing response can be modulated by modifying the input gate voltage.[32] To this end, the work functions (WFs), a parameter to evaluate the difficulty to release electrons from the surface to the vacuum level, of the Rh−ZnO monolayer before and after gas adsorption are calculated, as exhibited in Figure 5.

One can see from Figure 5 that the WF of the isolated Rh−ZnO monolayer is calculated to be 4.90 eV. Besides, the WF of the pristine ZnO monolayer according to our calculations is obtained as 5.44 eV. These findings exhibit that Rh-doping can largely reduce the WF of the pristine ZnO monolayer, thus
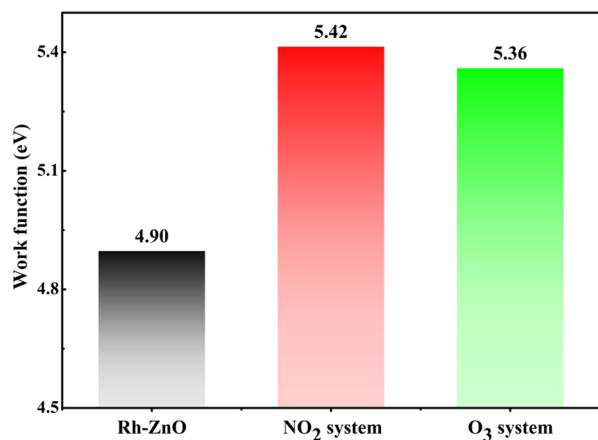

Figure 5. WF of the Rh−ZnO monolayer upon gas adsorption.

decreasing the electron affinity of the ZnO system, which would be beneficial for the Rh−ZnO monolayer to release electrons from its surface and enhance the charge transfer when interacting with impurity species.[33] After gas adsorption, the WF of the Rh−ZnO monolayer increases to 5.42 and 5.36 eV in the NO_2 and O_3 systems, respectively. That is, the adsorption of NO_2 can exert a larger impact on the WF of the Rh−ZnO monolayer, even though Q_T in this system is not as large as that in the O_3 system. Therefore, the following two findings could be identified: (i) the Rh−ZnO monolayer is a promising candidate for application as a field-effect transistor gas sensor with desirable sensing responses for NO_2 and O_3 detection and (ii) the Rh−ZnO monolayer can show much higher sensitivity upon NO_2 detection compared with O_3.

3. CONCLUSIONS

In this work, we use the first-principles theory to investigate the potential of the Rh−ZnO monolayer as a gas sensor for the detection of NO_2 and O_3 to evaluate the operation status of the ring main unit. The Rh dopant is stably anchored on the T_O site of the pristine ZnO surface with an E_b of 1.72 eV. The chemisorption is identified for NO_2 and O_3 adsorption with E_{ad} values of −2.11 and −1.35 eV, and Q_T values of −0.225e and −0.259e, respectively. In terms of the potential of the Rh−ZnO monolayer for NO_2 and O_3 detection, the BS analysis suggests its exploration as a resistance-type sensor with a higher response to O_3, while the WF analysis suggests its exploration as a field-effect transistor sensor with a higher response to NO_2. Our calculations would be beneficial for proposing novel sensing materials for application in the field of electrical engineering to guarantee the safe operation of the power system.

4. COMPUTATIONAL DETAILS

In this project, we employed the DMol3 package to perform the whole first-principles calculations,[34] wherein the spin-polarized calculations were employed with a self-consistent loop energy of 10^{-6} Ha, a global orbital cutoff radius of 5.0 Å, and a smearing of 0.005 Ha to ensure the good accuracy of the obtained energy.[35] The Perdew−Burke−Ernzerhof (PBE) functional within the generalized gradient approximation (GGA) was adopted to deal with the electron exchange-correlation terms.[36] The DFT-D2 method developed by Grimme was used to consider the van der Waals force and long-range interactions.[37] Double numerical plus polarization (DNP) was selected as the atomic orbital basis set.[38] A Monkhorst−Pack k-point mesh of $10 \times 10 \times 1$ was sampled for supercell calculations of geometric optimization and electronic properties.[39] The energy tolerance accuracy, maximum force, and displacement were set as 10^{-5} Ha, 2×10^{-3} Ha/Å, and 5×10^{-3} Å, respectively.[40]

We established a $4 \times 4 \times 1$ supercell for the ZnO monolayer with a vacuum region of 15 Å to perform simulations to prevent the possible interaction between the adjacent units.[41] The binding energy (E_b) was defined to reflect the binding strength between the Rh dopant and the ZnO surface as follows

$$E_b = E_{Rh-ZnO} - E_{ZnO} - E_{Rh} \tag{2}$$

where E_{Rh-ZnO}, E_{ZnO}, and E_{Rh} represent the total energy of the Rh−ZnO monolayer, pristine ZnO monolayer, and isolated Rh atom, respectively. Besides, the adsorption energy (E_{ad}) was

defined to evaluate the adsorption strength between the Rh−ZnO surface and the gas species as follows

$$E_{ad} = E_{Rh-ZnO/gas} - E_{Rh-ZnO} - E_{gas} \quad (3)$$

where $E_{Rh-ZnO/gas}$, E_{Rh-ZnO}, and E_{gas} represent the total energies of the gas adsorbed system, isolated Rh−ZnO monolayer, and gas molecule, respectively. Moreover, we applied the Hirshfeld method to analyze the charge of the Rh dopant (Q_{Rh}) in the Rh-doping process and the charge of the adsorbed gas (Q_T) in the gas adsorption systems.[42]

■ AUTHOR INFORMATION

Corresponding Author

Tian Wu − *School of Electrical Engineering & New Energy, China Three Gorges University, Yichang 443002, China;* orcid.org/0000-0003-1851-9786; Email: wutian_08@163.com

Authors

Yan Wang − *Foshan Power Supply Bureau of Guangdong Power Grid Corporation, Foshan 528000, China*

Xin Yang − *Foshan Power Supply Bureau of Guangdong Power Grid Corporation, Foshan 528000, China*

Cong Hu − *Foshan Power Supply Bureau of Guangdong Power Grid Corporation, Foshan 528000, China*

Complete contact information is available at:
https://pubs.acs.org/10.1021/acsomega.1c01439

Notes

The authors declare no competing financial interest.

■ ACKNOWLEDGMENTS

■ REFERENCES

(1) Wagenaars, P.; Wouters, P. A. A. F.; van der Wielen, P. C. J. M.; Steennis, E. F. Influence of Ring Main Units and Substations on Online Partial-Discharge Detection and Location in Medium-Voltage Cable Networks. *IEEE Trans. Power Delivery* 2011, 26, 1064−1071.

(2) Yoshida, T.; Koga, H.; Harada, T.; Miki, S.; Arioka, M.; Sato, S.; Yoshida, S.; Inoue, N.; Maruyama, A.; Takeuchi, T. Insulation Technology in Dry Air and Vacuum for a 72kV Low Pressured Dry Air Insulated Switchgear. *IEEJ Trans. Power Energy* 2008, 128, 1439−1444.

(3) Wagenaars, P.; Wouters, P. A. A. F.; van der Wielen, P. C. J. M.; Steennis, E. F. Influence of Ring Main Units and Substations on Online Partial-Discharge Detection and Location in Medium-Voltage Cable Networks. *IEEE Trans. Power Delivery* 2011, 26, 1064−1071.

(4) Chen, W.; Gui, Y.; Li, T.; Zeng, H.; Xu, L.; Ding, Z. Gas-sensing properties and mechanism of Pd-GaNNTs for air decomposition products in ring main unit. *Appl. Surf. Sci.* 2020, 531, No. 147293.

(5) Li, X.; Zhao, H.; Murphy, A. B. SF6-alternative gases for application in gas-insulated switchgear. *J. Phys. D: Appl. Phys.* 2018, 51, No. 153001.

(6) Cui, H.; Zhang, X.; Chen, D.; Tang, J. Adsorption mechanism of SF6 decomposed species on pyridine-like PtN3 embedded CNT: A DFT study. *Appl. Surf. Sci.* 2018, 447, 594−598.

(7) Srivastava, R.; Suman, H.; Shrivastava, S.; Srivastava, A. DFT analysis of pristine and functionalized zigzag CNT: A case of H2S sensing. *Chem. Phys. Lett.* 2019, 731, No. 136575.

(8) Gui, Y.; Li, W.; He, X.; Ding, Z.; Tang, C.; Xu, L. Adsorption properties of pristine and Co-doped TiO2 (1 0 1) toward dissolved gas analysis in transformer oil. *Appl. Surf. Sci.* 2020, 507, No. 145163.

(9) Cui, H.; Zhang, X.; Zhang, J.; Zhang, Y. Nanomaterials-based gas sensors of SF6 decomposed species for evaluating the operation status of high-voltage insulation devices. *High Voltage* 2019, 4, 242−258.

(10) Cao, W.; Gui, Y.; Chen, T.; Xu, L.; Ding, Z. Adsorption and gas-sensing properties of Pt2−GaNNTs for SF6 decomposition products. *Appl. Surf. Sci.* 2020, 524, No. 146570.

(11) Fan, Y.; Zhang, J.; Qiu, Y.; Zhu, J.; Zhang, Y.; Hu, G. A DFT study of transition metal (Fe, Co, Ni, Cu, Ag, Au, Rh, Pd, Pt and Ir)-embedded monolayer MoS2 for gas adsorption. *Comput. Mater. Sci.* 2017, 138, 255−266.

(12) Yang, A.; Pan, J.; Wang, D.; Lan, T.; Liu, Z.; Yuan, H.; Chu, J.; Wang, X.; Rong, M. Tunable SO2-sensing performance of arsenene induced by Stone-Wales defects and external electric field. *Appl. Surf. Sci.* 2020, 523, No. 146403.

(13) Zhang, W.; Yin, J.; Ding, Y.; Jiang, Y.; Zhang, P. Strain-engineering tunable electron mobility of monolayer IV−V group compounds. *Nanoscale* 2018, 10, 16750−16758.

(14) Cui, H.; Liu, T.; Zhang, Y.; Zhang, X. Ru-InN Monolayer as a Gas Scavenger to Guard the Operation Status of SF6 Insulation Devices: A First-Principles Theory. *IEEE Sens. J.* 2019, 19, 5249−5255.

(15) Gui, Y.; Shi, J.; Yang, P.; Li, T.; Tang, C.; Xu, L. Platinum modified MoS2 monolayer for adsorption and gas sensing of SF6 decomposition products: A DFT study. *High Voltage* 2020, 5, 454−462.

(16) Rao, G. S.; Hussain, T.; Islam, M. S.; Sagynbaeva, M.; Gupta, D.; Panigrahi, P.; Ahuja, R. Adsorption mechanism of graphene-like ZnO monolayer towards CO2 molecules: enhanced CO2 capture. *Nanotechnology* 2016, 27, No. 015502.

(17) Ma, D.; Wang, Q.; Li, T.; Tang, Z.; Yang, G.; He, C.; Lu, Z. CO catalytic oxidation on Al-doped graphene-like ZnO monolayer sheets: a first-principles study. *J. Mater. Chem. C* 2015, 3, 9964−9972.

(18) Meng, R.; Lu, X.; Ingebrandt, S.; Chen, X. Adsorption of Gas Molecules on Graphene-Like ZnO Nanosheets: The Roles of Gas Concentration, Layer Number, and Heterolayer. *Adv. Mater. Interfaces* 2017, 4, No. 1700647.

(19) Han, S. S.; Lee, H. M. Adsorption properties of hydrogen on (10,0) single-walled carbon nanotube through density functional theory. *Carbon* 2004, 42, 2169−2177.

(20) Luna, C. R.; Verdinelli, V.; German, E.; Seitz, H.; Volpe, M. A.; Pistonesi, C.; Jasen, P. V. Hydrogen Adsorption and Associated Electronic and Magnetic Properties of Rh-decorated (8,0) CNT Using Density Functional Theory. *J. Phys. Chem. C* 2015, 119, 13238−13247.

(21) Wan, Q.; Xu, Y.; Chen, X.; Xiao, H. Exhaled gas detection by a novel Rh-doped CNT biosensor for prediagnosis of lung cancer: a DFT study. *Mol. Phys.* 2018, 116, 2205−2212.

(22) Zhao, J. X.; Ding, Y. H. Theoretical study of the interactions of carbon monoxide with Rh-decorated (8,0) single-walled carbon nanotubes. *Mater. Chem. Phys.* 2008, 110, 411−416.

(23) Zhou, Q.; Zhang, G.; Tian, S.; Zhang, X. First-Principles Insight into Pd-Doped ZnO Monolayers as a Promising Scavenger for Dissolved Gas Analysis in Transformer Oil. *ACS Omega* 2020, 5, 17801−17807.

(24) Li, P.; Hong, Q.; Wu, T.; Cui, H. SOF2 sensing by Rh-doped PtS2 monolayer for early diagnosis of partial discharge in SF6 insulation device. *Mol. Phys.* 2021, No. e1919774.

(25) Cui, H.; Zhang, G.; Zhang, X.; Tang, J. Rh-doped MoSe2 as toxic gas scavenger: A first-principles study. *Nanoscale Adv.* 2019, 1, 772−780.

(26) Cui, H.; Jia, P. Doping effect of small Rhn (n = 1−4) clusters on the geometric and electronic behaviors of MoS2 monolayer: A first-principles study. *Appl. Surf. Sci.* 2020, 526, No. 146659.

(27) Murphy, L. R.; Meek, T. L.; Allred, A. L.; Allen, L. C. Evaluation and test of pauling's electronegativity scale. *J. Phys. Chem. A* 2000, 104, 5867−5871.

(28) Ji, Y.; Liu, Y.; Xu, Y.; Liu, L.; Chen, Y. Electronic and optical properties of sulfur vacancy-defect monolayer PtS2: A first-principles study. *Mater. Chem. Phys.* 2020, 255, No. 123588.

(29) Zhang, D.; Li, Q.; Li, P.; Pang, M.; Luo, Y. Fabrication of Pd-decorated MoSe 2 nanoflowers and density functional theory simulation toward ammonia sensing. *IEEE Electron Device Lett.* **2019**, *40*, 616−619.

(30) Ghobadi, N.; Touski, S. B. The electrical and spin properties of monolayer and bilayer Janus HfSSe under vertical electrical field. *J. Phys.: Condens. Matter* **2020**, *33*, No. 085502.

(31) Ma, D.; Jing, Z.; Li, X.; He, C.; Lu, Z.; Lu, Z.; Yang, Z.; Wang, Y. C3N monolayers as promising candidates for NO2 sensors. *Sens. Actuators, B* **2018**, 664−673.

(32) Huo, N.; Yang, S.; Wei, Z.; Li, S. S.; Xia, J. B.; Li, J. Photoresponsive and Gas Sensing Field-Effect Transistors based on Multilayer WS2 Nanoflakes. *Sci. Rep.* **2015**, *4*, No. 5209.

(33) Yu, Y. J.; Zhao, Y.; Ryu, S.; Brus, L. E.; Kim, K. S.; Kim, P. Tuning the graphene work function by electric field effect. *Nano Lett.* **2009**, *9*, 3430−3434.

(34) Delley, B. J. From molecules to solids with the DMol3 approach. *J. Chem. Phys.* **2000**, *113*, 7756−7764.

(35) Ju, W.; Li, T.; Su, X.; Li, H.; Li, X.; Ma, D. Au cluster adsorption on perfect and defective MoS2 monolayers: structural and electronic properties. *Phys. Chem. Chem. Phys.* **2017**, *19*, 20735−20748.

(36) Cui, H.; Jia, P.; Peng, X. Adsorption of SO2 and NO2 molecule on intrinsic and Pd-doped HfSe2 monolayer: A first-principles study. *Appl. Surf. Sci.* **2020**, *513*, No. 145863.

(37) Tkatchenko, A.; DiStasio, R. A., Jr.; Head-Gordon, M.; Scheffler, M. Dispersion-corrected Møller-Plesset second-order perturbation theory. *J. Chem. Phys.* **2009**, *131*, No. 094106.

(38) Cui, H.; Zhang, X.; Li, Y.; Chen, D.; Zhang, Y. First-principles insight into Ni-doped InN monolayer as a noxious gases scavenger. *Appl. Surf. Sci.* **2019**, *494*, 859−866.

(39) Monkhorst, H. J.; Pack, J. D. Special points for Brillouin-zone integrations. *Phys. Rev. B* **1976**, *13*, 5188−5192.

(40) Cui, H.; Chen, D.; Zhang, Y.; Zhang, X. Dissolved gas analysis in transformer oil using Pd catalyst decorated MoSe2 monolayer: A first-principles theory. *Sustainable Mater. Technol.* **2019**, *20*, No. e00094.

(41) Cui, H.; Jia, P.; Peng, X.; Li, P. Adsorption and sensing of CO and C2H2 by S-defected SnS2 monolayer for DGA in transformer oil: A DFT study. *Mater. Chem. Phys.* **2020**, *249*, No. 123006.

(42) Chen, D.; Zhang, X.; Tang, J.; Cui, Z.; Cui, H. Pristine and Cu decorated hexagonal InN monolayer, a promising candidate to detect and scavenge SF6 decompositions based on first-principle study. *J. Hazard. Mater.* **2019**, *363*, 346−357.